The Journal of Chemical Physics

Multi-scale simulation of the adsorption of lithium ion on graphite surface: From quantum Monte Carlo to molecular density functional theory

Cite as: J. Chem. Phys. **156**, 094709 (2022); https://doi.org/10.1063/5.0082944
Submitted: 20 December 2021 • Accepted: 15 February 2022 • Accepted Manuscript Online: 15 February 2022 • Published Online: 07 March 2022

Michele Ruggeri, Kyle Reeves, Tzu-Yao Hsu, et al.

The Journal of Chemical Physics ARTICLE scitation.org/journal/jcp

Multi-scale simulation of the adsorption of lithium ion on graphite surface: From quantum Monte Carlo to molecular density functional theory

Cite as: J. Chem. Phys. 156, 094709 (2022); doi: 10.1063/5.0082944
Submitted: 20 December 2021 • Accepted: 15 February 2022 •
Published Online: 7 March 2022

Michele Ruggeri,[1] Kyle Reeves,[1] Tzu-Yao Hsu,[2] Guillaume Jeanmairet,[2] Mathieu Salanne,[1,2,3,a)] and Carlo Pierleoni[1,4,b)]

AFFILIATIONS

[1] Maison de la Simulation, CEA, CNRS, Univ. Paris-Sud, UVSQ, Université Paris-Saclay, 91191 Gif-sur-Yvette, France
[2] Sorbonne Université, CNRS, Physicochimie des Électrolytes et Nanosystèmes Interfaciaux, F-75005 Paris, France
[3] Institut Universitaire de France (IUF), 75231 Paris, France
[4] Department of Physical and Chemical Sciences, University of L'Aquila, Via Vetoio 10, I-67010 L'Aquila, Italy

Note: This paper is part of the JCP Special Topic on Beyond GGA Total Energies for Solids and Surfaces.
[a)] **Electronic mail:** mathieu.salanne@sorbonne-universite.fr
[b)] **Author to whom correspondence should be addressed:** carlo.pierleoni@aquila.infn.it

ABSTRACT

The structure of the double-layer formed at the surface of carbon electrodes is governed by the interactions between the electrode and the electrolyte species. However, carbon is notoriously difficult to simulate accurately, even with well-established methods such as electronic density functional theory and molecular dynamics. Here, we focus on the important case of a lithium ion in contact with the surface of graphite, and we perform a series of reference quantum Monte Carlo calculations that allow us to benchmark various electronic density functional theory functionals. We then fit an accurate carbon–lithium pair potential, which is used in molecular density functional theory calculations to determine the free energy of the adsorption of the ion on the surface in the presence of water. The adsorption profile in aqueous solution differs markedly from the gas phase results, which emphasize the role of the solvent on the properties of the double-layer.

I. INTRODUCTION

Carbon materials play a very important role in many chemistry fields, ranging from catalysis to electrochemistry. In energy storage applications, carbon is used as an electrode in the form of graphite for Li-ion batteries,[1] of hard carbon for Na-ion batteries,[2] and of nanoporous materials for supercapacitors.[3] In all these examples, the carbon materials are put in contact with a charged electrolyte, and the interfacial structure and dynamics play a crucial role in the operation of the devices.[4,5] In order to optimize the performance, molecular simulations can play an important role,[6] but they need to accurately account for the interactions between the ions and the carbon surface.

Over the years, a large number of electronic density functional theory (eDFT) and molecular dynamics (MD) simulations were devoted to the study of electrochemical interfaces between carbon and ions or liquid electrolytes. Although they provide qualitatively similar results, some discrepancies may be observed when analyzing quantitative properties, such as adsorption energies, preferential "binding" distances, or adsorption profiles. For example, as reported by Valencia *et al.*,[7] in the case of bare lithium adsorption on graphite surfaces, eDFT calculations always display binding energies larger than 1 eV with a preference for the center of the C_6 hexagonal rings (hollow sites) with respect to adsorption above C atoms (top sites) or C–C bonds (bridge sites).[7] The lithium atom loses a valence electron, which is entirely transferred to the carbon surface. Yet, the adsorption energy may differ by more than 0.5 eV when changing the exchange-correlation functional.[8] In particular, the inclusion of the dispersion effect further increases the binding energy of the lithium ion.[9]

Similar problems arise in classical MD simulations due to the choice of different interaction potentials. On one hand, the choice of

the electrostatic model for the electrode atoms, which can be treated using fixed-charges or the constant potential method,[10] will impact the localization of the charge induced by the ions on the carbon. On the other hand, several force fields may be used for the short-range repulsion and dispersion interactions.

Important discrepancies were already reported in the case of the adsorption of water molecules on carbon surfaces.[5] In two studies on carbon nanotubes[11] and other carbon nanostructures,[12] Michaelides and co-workers compared the results of eDFT calculations using a large set of exchange-correlation functionals with diffusion Monte Carlo (DMC) calculations. DMC is a Quantum Monte Carlo (QMC) method, which explicitly accounts for electronic correlation and exchange. Although for fermions the fixed node error prevents DMC from being exact, it is more accurate than eDFT and belongs to the class of variational methods that can be systematically improved with enough effort. This method is much more costly than conventional eDFT in terms of computational time, but it is expected to capture the intermolecular interactions with a high accuracy. It can thus be viewed as a good reference for benchmarking purposes. Based on these results,[11,12] it appears that the choice of the exchange-correlation (XC) approximation in eDFT is crucial, but also that it is difficult to predict the accuracy since the adsorption energy results from a subtle balance of the interactions, especially at a medium range.

In this work, we follow a similar approach for the adsorption of lithium on graphite. The choice of the system was made based on its relevance for energy applications and because the lithium ions have a small number of valence electrons, thus allowing the cost of the reference DMC calculations. We computed the adsorption profiles on hollow, top and bridge sites by varying the distance between the lithium and the carbon material. DMC results are then compared with several XC approximations.

Yet, knowing the adsorption energy of a single ion may not be enough. Indeed, the solvent molecules within the electrolyte will also interact strongly both with the surface and with the ions, which can result in large variations of the adsorption properties under realistic conditions.[13] The main quantity to be determined is then the free energy of the adsorption profile, which should be obtained by sampling the whole liquid degrees of freedom. This quantity is not accessible to electronic structure methods due to their large computational cost, and it is necessary to resort to classical mechanics-based methods instead. Classical MD is usually the method of choice for such purposes, but it suffers from high inefficiency for systems studied under large dilution conditions. In such cases, it may conveniently be replaced by molecular DFT (MDFT). MDFT describes a liquid by its density field, and a functional of this density is introduced to account for entropic, external, and solvent–solvent interactions. The external contribution arises from the species in contact with the liquid, which are the graphite electrode and the lithium ion in the present study. The equilibrium density and its related free energy are computed through a variational procedure, which reduces the computational cost by several orders of magnitude with respect to atomistic MD. Recently, we have extended the MDFT method to account for constant potential electrodes, and we showed that it provides the correct structure and thermodynamics for liquid water in contact with graphite electrodes.[14]

In the second step of the present work, we build upon these developments to study the adsorption of lithium on graphite, in the presence of liquid water. The lithium–carbon interaction is parameterized using the electronic DFT calculations benchmarked on DMC. We show that the energy minimum observed in vacuum vanishes in the presence of the solvent, and that the lithium ion does not show anymore a preferred binding distance close to the surface due to the presence of water molecules.

II. COMPUTATIONAL METHODS

A. Quantum Monte Carlo

QMC simulations are a set of stochastic computational methods for the evaluation of observables of quantum systems. The fundamental idea behind these techniques is that expectation values of physical quantities of quantum systems can be written as

$$\langle A \rangle = \int d\mathbf{R}\, \Psi^*(\mathbf{R}) \hat{A} \Psi(\mathbf{R}), \tag{1}$$

where $\hat{A}$ is a generic observable, $\Psi(\mathbf{R})$ is the (normalized) wave function for the quantum system under analysis, and $\mathbf{R}$ represents the $3N$-dimensional electronic coordinate. The integral in Eq. (1) can then be evaluated using a Monte Carlo sampling.[15] A Markov chain Monte Carlo simulation consists of sampling a collection of configurations of the system used to estimate configurational integrals such as the one in Eq. (1).

In order to obtain meaningful information on the physical system, it is important to use a proper wave function. Since the exact ground state for physical systems of interest is unknown, it is necessary to guess the form of the ground state wave functions. A large variety of QMC methods exists, implementing different strategies. In this study, two QMC techniques were used, variation Monte Carlo (VMC) and DMC, using the fixed-node approximation.

In VMC, we approximate the ground state of the system by defining a trial wave function $\Psi_T(\mathbf{p};\ \mathbf{R})$, which is then plugged in Eq. (1); the resulting integral is then computed using a generalized Metropolis sampling. The trial wave function has a functional form that is chosen by taking into account the physical features of the system and depends on a set of variational parameters $\mathbf{p}$, which are optimized to obtain an approximation of the exact ground state. To optimize the trial wave function, we use the variational principle in quantum mechanics: for any given Hamiltonian, the ground state has, by definition, the lowest possible energy. What is done, in practice, is computing the energy using the trial wave function

$$\begin{aligned} E_{\mathbf{p}} &= \int d\mathbf{R}\, \Psi_T^*(\mathbf{p};\mathbf{R}) \hat{H} \Psi_T(\mathbf{p};\mathbf{R}) \\ &= \int d\mathbf{R}\, |\Psi_T(\mathbf{p};\mathbf{R})|^2 E_{loc}(\mathbf{p};\mathbf{R}), \end{aligned} \tag{2}$$

where we used the local energy $E_{loc}(\mathbf{p};\ \mathbf{R})$ defined as

$$E_{loc}(\mathbf{p};\mathbf{R}) = \frac{\hat{H}\Psi_T(\mathbf{p};\mathbf{R})}{\Psi_T(\mathbf{p};\mathbf{R})}. \tag{3}$$

By varying the parameters $\mathbf{p}$, we can minimize the energy $E_{\mathbf{p}}$, thus finding an approximation of the exact ground state within the chosen class of the trial functions. Another property that is used in wave function optimization is the zero-variance principle: for a given Hamiltonian, the energy variance of each energy eigenstate is zero. In order to use both the variational and the zero-variance principles,

the quantity that is optimized in practice is a linear combination of the energy and its variance.

While VMC allows estimates of ground state properties starting from a relatively simple trial wave function, VMC results are typically not realistically accurate. In order to improve these results, projection methods have to be used. Projection methods are a class of QMC methods that use imaginary time evolution to filter out excited states contribution from the trial wave function, allowing accurate computation of ground state properties. While, in principle, projection techniques are exact, the fermionic sign problem in practice prevents the exact evaluation of quantum observables; to avoid the sign problem, the fixed-node approximation is used. With this approximation, the results will still be approximate, but they will remain variational and significantly more accurate than the ones obtained with VMC (i.e., the computed energies and energy variance will be lower).

Several different projection QMC methods exist. Among those, one of the most commonly used in electronic structure calculations is DMC. If we consider a wave function $\Psi(\mathbf{R})$, a Hamiltonian with a potential energy term $U(\mathbf{R})$, and we define the imaginary time as $\tau = it$ in atomic unit, we have

$$\hat{H}\Psi(\mathbf{R}) = -\frac{1}{2}\Delta\Psi(\mathbf{R}) + U(\mathbf{R})\Psi(\mathbf{R}) = \frac{\partial\Psi(\mathbf{R})}{\partial\tau}; \tag{4}$$

the basic idea at the foundation of DMC is that there is a strong analogy between the imaginary time Schrödinger equation and a diffusion equation (coming from the kinetic part of $\hat{H}$) with an additional branching term [from $U(\mathbf{R})$]. It is thus possible to simulate the imaginary time propagation by using the process of diffusion and branching of classical random walkers, initially distributed according to a trial wave function (obtained via the optimization procedure described above). The practical details of the implementation of DMC can be found in the literature.[16,17] The important things to stress here is that the accuracy of fixed-node DMC result depends on the accuracy of the nodal surface of the trial wave function, and that the results are variational with respect to the nodal location.

All QMC computations in the present work were performed using the QMCpack software.[18] We used QMC calculations to determine the adsorption energy of the Li atom adsorbed on a graphite substrate as a function of the separation between the Li atom and the surface. If z is the distance between the Li atom and the carbon surface, the adsorption energy profile $E_{ads}(z)$ is defined as

$$E_{ads}(z) = E_{\mathrm{Li+C}}(z) - (E_{\mathrm{Li}} + E_{\mathrm{C}}), \tag{5}$$

where $E_{\mathrm{Li+C}}(z)$ is the energy of a system made of a graphite substrate with a Li atom at a distance z and E_{Li} and E_{C} are the energy of the isolated atom and graphite, respectively. The latter is modeled using two graphene layers made of 50 C atoms each, with an AB stacking (which corresponds to a $5 \times 5 \times 1$ supercell). The energy profile was computed for three different setups: with the Li atom lying above the center of a C hexagon (hollow site), above a C atom (top site), and above a C–C bond (bridge site).

All simulations were done using a simulation box with cell parameters (in Å),

$$\begin{bmatrix} 12.336 & 0.000 & 0.000 \\ 6.168 & 10.683 & 0.000 \\ 0.000 & 0.000 & 30.000 \end{bmatrix}.$$

The height of the simulation box was selected after systematically testing the convergence of the total energy as a function of the amount of vacuum between periodic images in the z direction of the graphite bilayer using eDFT (see Sec. S1 in the supplementary material) using the Perdew–Burke–Ernzerhof (PBE) functional. Dispersion corrections[19] were then used to relax the carbon bilayer structure for the selected box height of 30 Å, yielding a distance between the two planes of 3.47 Å, which was used for the QMC computations. This value is slightly larger than the one provided in previous QMC studies (3.43 Å),[20,21] but this should not impact the computed adsorption energies. Previous investigations systematically studied convergence with the size of the supercell and the number of twists for single and bilayer systems.[20,21,28] Here, for computational reasons, we assumed the mentioned $5 \times 5 \times 1$ supercell and we used a $4 \times 4 \times 1$ twist grid (corresponding to eight nonequivalent twists)[22] based on the convergence of the corresponding DFT energy. Although convergence of the DFT total energy with the twist grid is reached only for an $8 \times 8 \times 1$ k-points grid, the residual effect is less than 1 mHa. Moreover, in the property we are aiming, namely, the absorption energy of the lithium atom, size effects should largely cancel since the same simulation cell and twist grid were used in all the simulations, including the ones of the isolated atom and substrate.

In all VMC and DMC simulations, we used the trial wave function with a Slater-Jastrow form

$$\Psi_T(\mathbf{p};\mathbf{R}) = J(\mathbf{p};\mathbf{R})D(\mathbf{R}), \tag{6}$$

where $J(\mathbf{p};\ \mathbf{R})$ is a Jastrow term describing electronic correlation, with one and two body terms, and $D(\mathbf{R})$ is a Slater determinant, ensuring the correct fermionic antisymmetry. The single particle orbitals used in the Slater determinant were evaluated using DFT with a PBE[23] functional. The orbital calculations were performed using the QUANTUM ESPRESSO software.[24,25] In the DFT calculations, a plane wave basis set was used, with a cutoff at 150 Ry, using norm conserving pseudopotentials for both the Li and C atoms. In QMC simulations, the Burkatzki–Dolg–Filippi set of pseudopotentials was used.[26] Wave function optimization is performed using the linear method[27] and iterated until the optimized energy converges. Only the Jastrow part of the trial wave function is optimized. More information on the Jastrow part of the trial wave function can be found in Sec. S2 in the supplementary material. We report DMC results obtained using an imaginary time step of $\tau = 0.01$ Ha^{-1} and a population of 12 000–16 000 random walkers. Previous QMC simulations of a similar system[28] showed that using these parameters leads to energies converged to a few mHa per atom. We also note that we are performing QMC simulations for a system whose size was deemed large enough to give an accurate description of Li in the proximity of carbon. Size consistent, non local T-moves[29] are used, as well as the ZSGMA branching scheme.[30]

B. Electronic density functional theory

Electronic DFT calculations were performed using the QUANTUM ESPRESSO electronic structure code.[24,25] To be

consistent with the QMC result, an identical simulation cell was considered, consisting of one hundred carbon atoms divided among two graphite layers with AB stacking (which corresponds to a 5 × 5 × 1 supercell). A kinetic energy cutoff of 40 Ry was used.

We compared the adsorption energy profiles for two series of XC functionals. In the first series, we used the local-density approximation (LDA),[31] PBE,[23] and BLYP,[32,33] which neglect the London dispersion interaction. Then, we included the latter using either the D2 correction parameterized by Grimme,[34] or through the use of the vdW-DF-C09 functional[35–37] implemented in the Libxc library.[38] Rappe–Rabe–Kaxiras–Joannopoulos ultrasoft (rrkjus) pseudopotentials[39] were used for both carbon and lithium atoms.

Several uniform Monkhorst–Pack grids of 1 × 1 × 1, 2 × 2 × 1, 3 × 3 × 1, and 5 × 5 × 1 k-points were tested for a single Li distance of 2.4 Å from the graphite surface (see the supplementary material, Sec. S3). The difference between the total energy of the 1 × 1 × 1 and 2 × 2 × 1 grids is roughly 26 meV, and thus, the 1 × 1 × 1 grid was used for the calculations throughout this work. Additionally, an extended system consisting of four carbon layers instead of two was simulated to check the effect of the number of graphite layers; almost no difference was observed for the absorption energy profile as shown in Sec. S4 in the supplementary material.

Similar to the QMC calculations, the lithium atom was systematically above the three adsorption sites. The energies were converged at each step to an accuracy of 1×10^{-6} Ry. To align the various curves, the non-interacting systems (i.e., graphite and lithium atom separately) were computed for each XC functional, and the binding energy was obtained according to Eq. (5).

C. Molecular density functional theory

Solvation free energies were computed with MDFT[14,40,41] while the polarizability of the graphite sheets was handled using the fluctuating Gaussian charges method.[14,42,43] MDFT is a flavor of classical density functional theory (cDFT) developed to study the solvation properties of molecular solutes into molecular solvents such as water or acetonitrile. The solvent is described by its density field $\rho(\boldsymbol{r},\boldsymbol{\omega})$, which measures the average number per unit volume of molecules with an orientation $\boldsymbol{\omega}$ at a given position $\boldsymbol{r}$. The solute acts as a perturbation through an external potential $V_{\text{ext}}(\boldsymbol{r},\boldsymbol{\omega})$ causing the solvent to deviate from the homogeneous bulk fluid.

According to the cDFT principles,[44,45] there exists a unique functional, F, of the solvent density, ρ, that is equal to the solvation free energy at its minimum, which is reached for the equilibrium solvent density. To find an expression for the functional, a common practice is to start by splitting it into the following sum:

$$F[\rho(\boldsymbol{r},\boldsymbol{\omega})] = F_{\text{id}}[\rho(\boldsymbol{r},\boldsymbol{\omega})] + F_{\text{exc}}[\rho(\boldsymbol{r},\boldsymbol{\omega})] + \iint \rho(\boldsymbol{r},\boldsymbol{\omega}) V_{\text{ext}}(\boldsymbol{r},\boldsymbol{\omega}) d\boldsymbol{r} d\boldsymbol{\omega}. \quad (7)$$

In Eq. (7), the first term of the rhs is called ideal and corresponds to the entropic contribution of a non-interacting fluid with the same density. The second term is due to the solvent–solvent interaction and is often called the excess term while the last term is due to the solute–solvent interaction, and thus, called the external term.

Exact expressions exist for the ideal and external functionals that can be computed numerically. The excess part, however, requires approximations. It can be expressed as an infinite Taylor expansion around the homogeneous bulk solvent density ρ_b,

$$F_{\text{excess}}[\rho] = -\frac{k_B T}{2} \iiiint \Delta\rho(\boldsymbol{r},\boldsymbol{\omega}) c^{(2)}(\boldsymbol{r}-\boldsymbol{r}',\boldsymbol{\omega},\boldsymbol{\omega}') \times \Delta\rho(\boldsymbol{r}',\boldsymbol{\omega}') d\boldsymbol{r} d\boldsymbol{\omega} d\boldsymbol{r}' d\boldsymbol{\omega}' + F_B[\rho]. \quad (8)$$

In Eq. (8), $\Delta\rho(\boldsymbol{r},\boldsymbol{\omega}) = \rho(\boldsymbol{r},\boldsymbol{\omega}) - \rho_b$, k_B is the Boltzmann constant, T is the temperature, and $c^{(2)}$ is the two-body direct correlation function of bulk solvent. F_B is the so-called bridge functional that collects all the terms higher than quadratic, involving many-body direct correlation functions of the bulk solvent. A common way to approximate the excess functional is to ignore the bridge functional, i.e., $F_B = 0$, resulting to the "HNC" functional because it is equivalent to using the hypernetted chain (HNC) closure for the solute–solvent correlations in the molecular Ornstein–Zernike equation.[41] In this work, we use a very simple bridge functional[46,47] based on weighted density approximation that is known to correct well for the dramatic pressure overestimation of the HNC approximation. Water is modeled with the three-sites extended Simple Point Charge (SPC/E) force field[53] while the external potential V_{ext} is created by the graphite electrodes and the lithium ion whose interactions are described as the sum of Lennard-Jones and electrostatic interactions. The Lennard-Jones and charge parameters of the four types of atoms involved are collected in Table I. For the carbon atoms, the choice of the force field of Werder *et al.*[48] was made based on a previous QMD study, in which it was shown to provide a good estimate of the energy of adsorption of a water molecule on a graphene surface.[11]

The electrode charges are represented with Gaussian charge distributions with a width of 0.40 Å. These partial charges are calculated by enforcing a uniform potential within the whole carbon electrode, with an overall electroneutrality constraint (hence forcing the total charge on the carbon to be equal to -e).[42] Electrode charges are optimized self consistently with the functional minimization through an iterative scheme.[14]

In the first step, the functional of Eq. (7) is minimized with no charges on the lithium and the carbon atoms. Then, carbon charges are optimized in the presence of the inhomogeneous water charge density and the lithium cation. The functional is minimized again but in the presence of lithium charge and the previously determined electrode charges. The process is repeated until it converges, with a convergence criterion of 5×10^{-4} on the relative change in solvation free energy between two consecutive steps.

MDFT calculations were performed using an in-house Fortran code and electrode charges are optimized using the constant

TABLE I. Force-field parameters used in the MDFT simulations. Mixed parameters are computed using the Lorentz–Berthelot rules (except for the C–Li interaction, which does not affect the MDFT results).

Atoms	σ (-Å)	ϵ (kJ/mol)	Charge (e)
O	3.166	0.65	−0.8476
H	0	0	0.4238
Li[49]	2.216	0.076 48	1
C[48]	3.214	0.236 4	Fluctuating

potential molecular dynamics software MetalWalls.[50] We use a $24.672 \times 21.366 \times 40$ Å^3 simulation box (the unit cell used in QMC is replicated twice in x and y directions) with $74 \times 64 \times 120$ grid nodes and an angular grid of 196 orientations per grid node. We run calculations for a distance z between the electrode plane and the lithium varying between $z = 1.0$ and $z = 10$ Å with an increment of 0.2 Å between 1 and 6 Å and of 0.5 Å otherwise.

III. RESULTS AND DISCUSSION

A. Benchmark of the DFT functionals with QMC

We first discuss the QMC results for the three adsorption sites. QMC total energies and adsorption energies are reported in Table II.

From Table II, it appears clearly that the adsorption energies are larger for the top and bridge sites than for the hollow site for distances of 1.5 and 2.0 Å in good agreement with previous eDFT results from the literature and from the current study. At a larger distance of 3.0 Å, the three sites display similar energies, which shows that the difference between them has a short-range character. Due to the high computational cost of DMC, further lithium–carbon distances were only considered for the hollow site. We obtained a binding energy E_b of −1.08 eV for a lithium–surface distance of 1.8 Å. We also observe a somewhat peculiar behavior since the adsorption energy is rather similar for distances of 3 and 4 Å. By analyzing the corresponding electronic densities as shown in Fig. 1(a), we observe that this corresponds to the region in which the electron transfer occurs. For distances lower than 3 Å, the energies correspond to the adsorption of a lithium ion on a polarized carbon surface, while for distances greater than 4 Å, the system corresponds to the neutral lithium atom and carbon material.

TABLE II. QMC energies for the adsorption of lithium on graphite for the three different sites for several lithium–carbon distances reported in the first column (in Å). The second column shows VMC results while the third column shows DMC results. The last column lists the adsorption energies computed with DMC using Eq. (5).

	E_{VMC} (Ha)	E_{DMC} (Ha)	E_{ads} (eV)
Graphite	−567.202 1(4)	−568.531(1)	···
Li atom	−0.198 050(9)	−0.198 314(3)	···
Hollow site			
1.0	−567.357 3(5)	−568.693(1)	0.98(4)
1.5	−567.429 7(4)	−568.763(1)	−0.92(5)
1.8	−567.434 1(4)	−568.769(1)	−1.08(5)
2.0	−567.431 3(5)	−568.768(1)	−1.06(4)
3.0	−567.400 6(5)	−568.742(1)	−0.35(4)
4.0	−567.401 1(4)	−568.741(1)	−0.32(5)
8.0	−567.393 5(4)	−568.730(2)	−0.03(6)
Top site			
1.5	−567.366 3(4)	−568.705(2)	0.65(5)
2.0	−567.422 6(4)	−568.761(1)	−0.87(4)
3.0	−567.400 5(5)	−568.740(2)	−0.31(4)
Bridge site			
1.5	−567.379 9(4)	−568.716(2)	0.36(4)
2.0	−567.425 1(4)	−568.760(1)	−0.83(3)
3.0	−567.399 9(4)	−568.742(1)	−0.35(3)

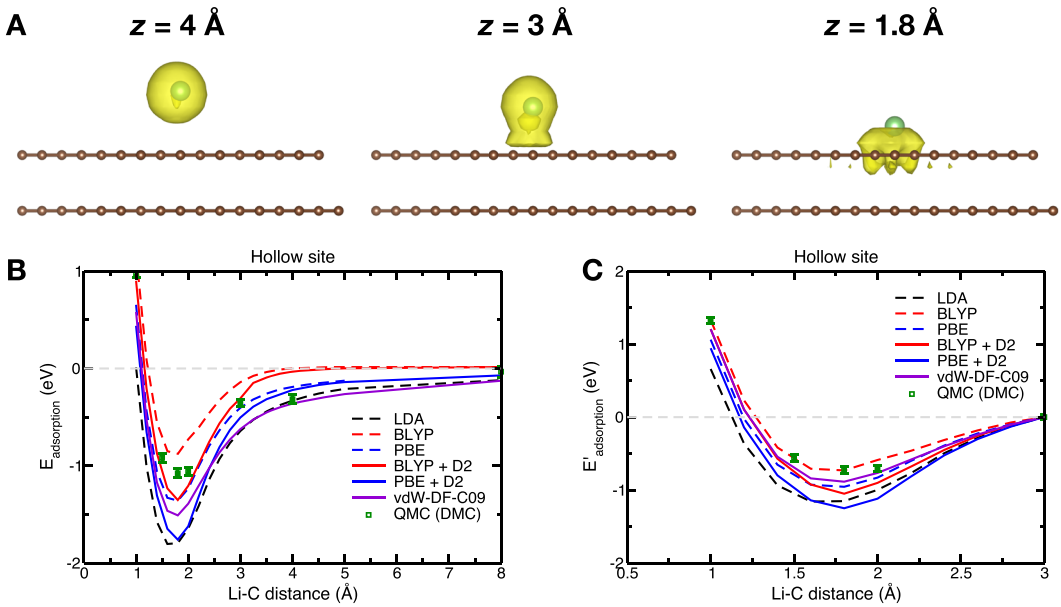

FIG. 1. (a) Electron density around a Li atom adsorbed on a graphite substrate, computed via quantum Monte Carlo, for different atom–substrate distances. The densities were obtained by computing the overall electronic density of a system with a Li atom adsorbed on graphite and subtracting the density of the isolated substrate, in the absence of the adsorbed atom. All shown isosurfaces correspond to a density of $6 \cdot 10^{-4}$ electrons/Å^3. (b) Comparison of the adsorption energies obtained with various DFT functionals and DMC for the adsorption of the lithium on the hollow site of graphite. (c) Same as (b) but subtracting the adsorption energy at a distance of 3 Å.

The adsorption profiles obtained for the hollow site for the LDA, BLYP, PBE, BLYP+D2, PBE+D2, and dW-DF-C09 functionals are compared with the DMC benchmark in Fig. 1(b). The LDA results in a strong overbinding, which is expected. The comparison with the other functionals is more surprising. The QMC results lie between the BLYP and the BLYP+D2, while all the other functionals predict too low adsorption energies. However, as noted by Valencia *et al.*, the binding energy (defined as the minimum of the adsorption energy profile) should be approximately given by[7]

$$E_b \approx E_b(\mathrm{Li}^+) - (IP[\mathrm{Li}] - W_f[\mathrm{Graphite}]), \tag{9}$$

where $E_b(\mathrm{Li}^+)$ is the binding energy of the lithium *ion*, IP is its ionization potential, and W_f is the work function of graphite. The observed variation may, therefore, be due to different values of IP and W_f from the various functionals.

By visualizing the electronic density of the system using various DFT functionals (see the supplementary material, Fig. S6), we also observe that they yield similar results to the QMC calculations up to 3 Å, while some discrepancies are observed at a larger distance of 4 Å. In the present work, we are mostly interested in developing an accurate potential for the adsorption of the lithium ion. Consequently, we performed a second comparison of the various functionals in which the energy at z = 3 Å is subtracted. The results are shown in Fig. 1(c). The discrepancy between the various functionals is somewhat lower. The best agreement is now obtained with the BLYP, PBE, and vdW-DF-C09 functionals, while the others predict overbinding. For the two former approximations, the good agreement may be fortuitous since they do not account for the dispersion effects. However, this points toward an overestimation of the dispersion effects when using the D2 correction. Indeed, in the case of the lithium ion, only two semi-core electrons take part in the interaction, which should result in a very weak dispersion term. The vdW-DF-C09 functional, which accounts for these effect explicitly and not through a parameterized term, seems to better catch the interactions.

B. Fitting the carbon–lithium potential

In order to incorporate solvent effects, it is necessary to develop accurate classical interaction potentials. It is not possible to fit them directly on the QMC calculations due to the limited amount of data. Instead, we pick the most accurate functional, vdW-DF-C09, and calculate the Li–graphite binding energy for a large number of distances. The intermolecular interaction should, in principle, account for four different effects: electrostatics, polarization, short-range repulsion, and dispersion. In our electrostatic model, the two former effects are explicitly introduced through the use of a +1 point charge on the lithium and of the calculation of partial (Gaussian) charges on the carbon atoms. These partial charges are calculated for each lithium–carbon distance using the same methodology as described in Sec. II C.

Concerning the short-range repulsion and the dispersion effects, the two main potentials used in the literature are the Lennard-Jones and the Born–Huggins–Mayer (BHM) ones. However, it appears that the electrostatic interaction was sufficient to account for the attractive part of the binding energy, as shown in Fig. 2. The fitted potential should, therefore, add very few, if no contribution for the dispersion interaction, which agrees with the previous observation on the use of dispersion-corrected functionals. A well-known drawback of the Lennard-Jones potential is that it is not possible to fit the short-range repulsion and the dispersion term separately since they both involve the same parameters. We have, therefore, chosen a BHM potential instead, the analytical form of which is

$$V_{\mathrm{BHM}}(r) = A\,\exp(-br) - \frac{C_6}{r^6}, \tag{10}$$

where A and b are the parameters describing the intensity and the range of the repulsion interaction, while C_6 is the dipole–dipole dispersion interactions. In principle, higher order terms could be included for dispersion, but as discussed above, this term is almost negligible in the case of the lithium ion. The fitted potential reproduces with a high accuracy the vdW-DF-C09 curves for the three types of absorption sites as shown in Fig. 2. It also matches very well with the BLYP (not shown in the figure) as well as the QMC results (on which it was not fitted) adsorption curves. The corresponding parameters are A = 91.17, b = 2.518, and C_6 = 1.107 (all numbers are given in atomic units).

C. Adsorption of the lithium ion in the presence of water

The fitted potential can directly be used in any classical molecular simulation, such as MD. Since we focus here on the

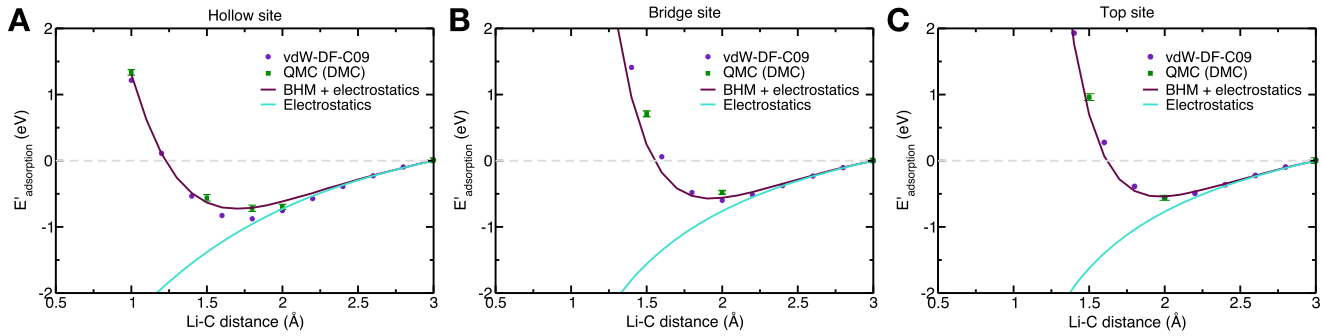

FIG. 2. Comparison of the fitted potential with the QMC and vdW-DF-C09 energies for the three different absorption sites. Panel (a): hollow site; panel (b): bridge site; panel (c): top site.

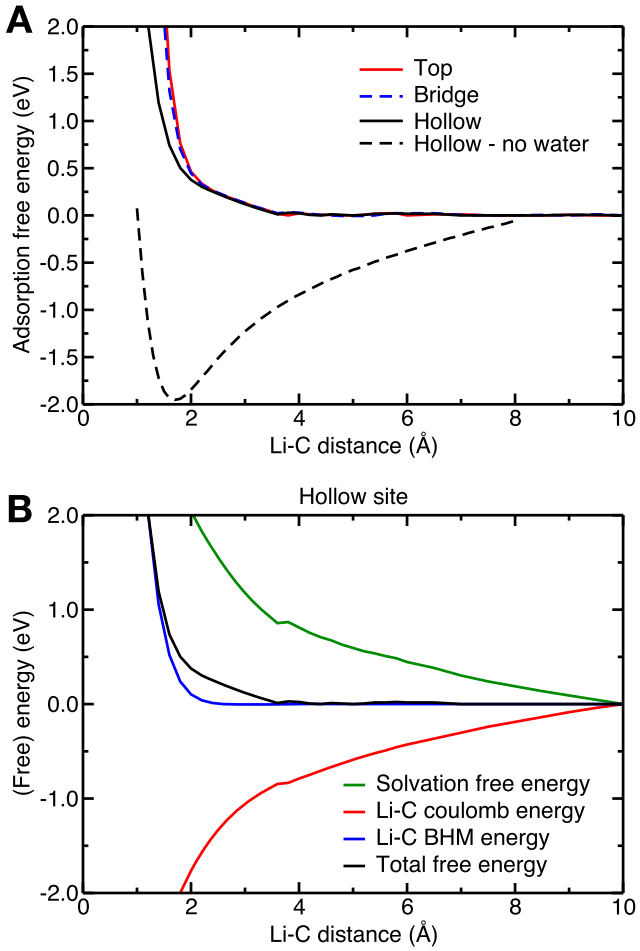

FIG. 3. (a) Adsorption free energy for a lithium ion on the graphite surface in the presence of water, computed using MDFT, for the three adsorption sites. The energy variation in the absence of water is also shown for comparison. (b) Contributions to the total free energy for the hollow adsorption site in the MDFT calculation.

adsorption free energy of the lithium ion on the carbon surface, we prefer to use MDFT, which is a computationally more efficient alternative. The solvation free energy of a single system can be computed within a few minutes on a single central processing unit (CPU), while it would require tens of CPU hours with MD. The free energy profiles obtained for the three adsorption sites in the presence of liquid water are shown in Fig. 3(a). The profiles are very different from the gas phase results. The minimum at ≈1.8 Å completely disappears and is replaced by a strongly repulsive wall. This shows that there is no preferential adsorption of lithium on the graphite surface in the aqueous phase.

This result is in qualitative agreement with a recent MD study on the adsorption of hydrated ions on graphene,[51] which provided a repulsive free energy profile over the whole range of considered distances. Yet, the latter study did not include any Coulombic interaction between the ion and the carbon surface, which is the main driving force for adsorption in the gas phase as discussed above. It is thus interesting to examine the various contributions to the total free energy, which are provided in Fig. 3(b). We observe that the electrostatic attraction between Li and C is, in fact, counterbalanced by the solvation free energy. The latter contains the electrostatic interactions of the water molecules with both the lithium and the graphite surface, which results in a strong screening effect. The extent of this screening effect was studied in detail in a recent study focused on gold surfaces:[52] the presence of the water molecules strongly impacts the polarization of the surface. Consequently, the total free energy is almost equal to the BHM contribution over the whole range of distances, except between 2 and 5 Å, where the solvation free energy overcomes the ion-surface Coulombic interaction, resulting in a more repulsive potential.

The effect of the solvent can be further analyzed by plotting the density profiles for various distances between the ion and the surface (Fig. 4). At z = 8 Å, two regions with larger densities emerge, corresponding to the surface adsorbed water molecules at a distance of 3 Å from the surface[14] on one hand and to the lithium ion first solvation shell on the other hand. At a distance of 5 Å, the solvation shell starts to overlap with the adsorbed layer at close contact to the electrode, which results in small depletion zones in the latter. These depletion zones remain observable at smaller distances, but the impact on the free energy becomes negligible with respect to the large short-range repulsion between the carbon and the lithium.

IV. CONCLUSION

Two main results were obtained in this work. First, we provide an accurate set of benchmark energies for the adsorption of lithium on a graphite surface, using an accurate QMC approach. These data can be used in future studies to test the accuracy of XC functionals

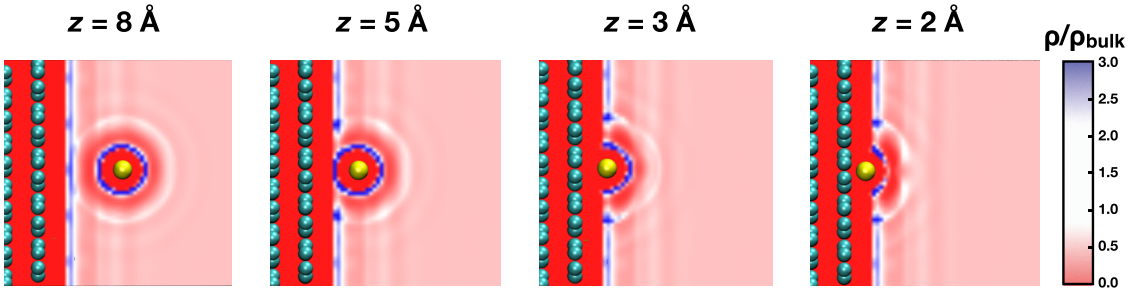

FIG. 4. Projection of the solvent densities computed using MDFT for various lithium–carbon distances.

for such important problems in surface science or to parameterize new force fields between the two species. Here, we obtained a very good agreement using a BHM potential, but different approaches may be proposed in the future. Second, we used the parameterized force field in order to compute the free energy profile for the adsorption of a lithium ion at the graphite surface in the presence of water as a solvent. MDFT was preferred over classical MD for this calculation due to its much lower computational cost. We showed that the low energy minimum obtained in the gas phase completely vanishes, resulting in an overall repulsive profile over the whole range of studied lithium–carbon distances. This is due to the screening of the attractive Coulombic term by the water molecules on the one hand and on the other hand to the interferences between the densities corresponding to the first adsorbed layer on carbon and to the first solvation shell of the cation.

The proposed multi-scale approach may be extended to a large variety of systems in the future. In particular, it would be interesting to study how adsorption varies within the alkali and alkali-earth cationic series. The study of larger organic ions would be very useful for the scope of supercapacitor devices, but this would require additional work to account accurately for the flexibility of the ion. Finally, the study of more polarizable electrode materials such as gold or platinum would be relevant in the context of catalysis. Changing metal would lead to very different adsorption properties for the solvent so that one can expect large differences in the adsorption free-energy profiles of ions at electrodes.

SUPPLEMENTARY MATERIAL

Technical details are provided in the supplementary material. It comprises five sections. Section S1 reports the convergence study with the height of the simulation box, Sec. S2 reports details about the Jastrow part of the QMC trial wave function, Sec. S3 is devoted to the convergence of the DFT energy with the k-point grid, Sec. S4 describes the influence of the number of carbon layers, and, finally, Sec. S5 reports the excess electronic density from two different DFT theories.

ACKNOWLEDGMENTS

This project received funding from the European Research Council (ERC) under the European Union's Horizon 2020 research and innovation program (Grant Agreement No. 771294). This work was granted access to the HPC resources of CINES under Allocation No. A0100910463 made by GENCI and benefited from the "Grand Challenge Jean Zay" program. We acknowledge support from EoCoE, a project funded by European Union Contract Nos. H2020-EINFRA-2015-1-676629 and H2020-INFRAEDI-2018-824158.

AUTHOR DECLARATIONS

Conflict of Interest

The authors declare no conflicts of interest.

DATA AVAILABILITY

The input files used in this study for the QMC, DFT, and classical simulations are openly available in the repository at https://gitlab.com/ampere2, together with the reference energies for the QMC calculations.

REFERENCES

[1] M. Armand and J.-M. Tarascon, "Building better batteries," Nature **451**, 652–657 (2008).
[2] X. Dou, I. Hasa, D. Saurel, C. Vaalma, L. Wu, D. Buchholz, D. Bresser, S. Komaba, and S. Passerini, "Hard carbons for sodium-ion batteries: Structure, analysis, sustainability, and electrochemistry," Mater. Today **23**, 87–104 (2019).
[3] P. Simon and Y. Gogotsi, "Capacitive energy storage in nanostructured carbon-electrolyte systems," Acc. Chem. Res. **46**, 1094–1103 (2013).
[4] M. Salanne, B. Rotenberg, K. Naoi, K. Kaneko, P.-L. Taberna, C. P. Grey, B. Dunn, and P. Simon, "Efficient storage mechanisms for building better supercapacitors," Nat. Energy **1**, 16070 (2016).
[5] A. Striolo, A. Michaelides, and L. Joly, "The carbon-water interface: Modeling challenges and opportunities for the water-energy nexus," Annu. Rev. Chem. Biomol. Eng. **7**, 533–556 (2016).
[6] E. H. Lahrar, P. Simon, and C. Merlet, "Carbon-carbon supercapacitors: Beyond the average pore size or how electrolyte confinement and inaccessible pores affect the capacitance," J. Chem. Phys. **155**, 184703 (2021).
[7] F. Valencia, A. H. Romero, F. Ancilotto, and P. L. Silvestrelli, "Lithium adsorption on graphite from density functional theory calculations," J. Phys. Chem. B **110**, 14832–14841 (2006).
[8] K. Rytkönen, J. Akola, and M. Manninen, "Density functional study of alkali-metal atoms and monolayers on graphite (0001)," Phys. Rev. B **75**, 075401 (2007).
[9] X. Fan, W. T. Zheng, J.-L. Kuo, and D. J. Singh, "Adsorption of single Li and the formation of small Li clusters on graphene for the anode of lithium-ion batteries," ACS Appl. Mater. Interfaces **5**, 7793–7797 (2013).
[10] L. Scalfi, M. Salanne, and B. Rotenberg, "Molecular simulation of electrode-solution interfaces," Annu. Rev. Phys. Chem. **72**, 189–212 (2021).
[11] Y. S. Al-Hamdani, D. Alfè, and A. Michaelides, "How strongly do hydrogen and water molecules stick to carbon nanomaterials?," J. Chem. Phys. **146**, 094701 (2017).
[12] J. G. Brandenburg, A. Zen, D. Alfè, and A. Michaelides, "Interaction between water and carbon nanostructures: How good are current density functional approximations?," J. Chem. Phys. **151**, 164702 (2019).
[13] C. Merlet, M. Salanne, B. Rotenberg, and P. A. Madden, "Influence of solvation on the structural and capacitive properties of electrical double layer capacitors," Electrochim. Acta **101**, 262–271 (2013).
[14] G. Jeanmairet, B. Rotenberg, D. Borgis, and M. Salanne, "Study of a water-graphene capacitor with molecular density functional theory," J. Chem. Phys. **151**, 124111 (2019).
[15] N. Metropolis, A. W. Rosenbluth, M. N. Rosenbluth, A. H. Teller, and E. Teller, "Equation of state calculations by fast computing machines," J. Chem. Phys. **21**, 1087–1092 (1953).
[16] W. M. C. Foulkes, L. Mitas, R. J. Needs, and G. Rajagopal, "Quantum Monte Carlo simulations of solids," Rev. Mod. Phys. **73**, 33–83 (2001).
[17] C. J. Umrigar, M. P. Nightingale, and K. J. Runge, "A diffusion Monte Carlo algorithm with very small time-step errors," J. Chem. Phys. **99**, 2865–2890 (1993).
[18] J. Kim, A. D. Baczewski, T. D. Beaudet, A. Benali, M. C. Bennett, M. A. Berrill, N. S. Blunt, E. J. L. Borda, M. Casula, D. M. Ceperley, S. Chiesa, B. K. Clark, R. C. Clay, K. T. Delaney, M. Dewing, K. P. Esler, H. Hao, O. Heinonen, P. R. C. Kent, J. T. Krogel, I. Kylänpää, Y. W. Li, M. G. Lopez, Y. Luo, F. D. Malone, R. M. Martin, A. Mathuriya, J. McMinis, C. A. Melton, L. Mitas, M. A. Morales, E. Neuscamman, W. D. Parker, S. D. P. Flores, N. A. Romero, B. M. Rubenstein, J. A. R. Shea, H. Shin, L. Shulenburger, A. F. Tillack, J. P. Townsend, N. M. Tubman, B. Van Der Goetz, J. E. Vincent, D. C. Yang, Y. Yang, S. Zhang, and L. Zhao, "QMCPACK: An open source *ab initio* quantum Monte Carlo package for the electronic structure of atoms, molecules and solids," J. Phys.: Condens. Matter **30**, 195901 (2018).

[19]S. Grimme, J. Antony, S. Ehrlich, and H. Krieg, "A consistent and accurate *ab initio* parametrization of density functional dispersion correction (DFT-D) for the 94 elements H–Pu," J. Chem. Phys. **132**, 154104 (2010).
[20]E. Mostaani, N. D. Drummond, and V. I. Fal'ko, "Quantum Monte Carlo calculation of the binding energy of bilayer graphene," Phys. Rev. Lett. **115**, 115501 (2015).
[21]H. Shin, J. Kim, H. Lee, O. Heinonen, A. Benali, and Y. Kwon, "Nature of interlayer binding and stacking of sp-sp^2 hybridized carbon layers: A quantum Monte Carlo study," J. Chem. Theory Comput. **13**, 5639–5646 (2017).
[22]C. Lin, F. H. Zong, and D. M. Ceperley, "Twist-averaged boundary conditions in continuum quantum Monte Carlo algorithms," Phys. Rev. E **64**, 016702 (2001).
[23]J. P. Perdew, K. Burke, and M. Ernzerhof, "Generalized gradient approximation made simple," Phys. Rev. Lett. **77**, 3865–3868 (1996).
[24]P. Giannozzi, S. Baroni, N. Bonini, M. Calandra, R. Car, C. Cavazzoni, D. Ceresoli, G. L. Chiarotti, M. Cococcioni, I. Dabo, A. Dal Corso, S. de Gironcoli, S. Fabris, G. Fratesi, R. Gebauer, U. Gerstmann, C. Gougoussis, A. Kokalj, M. Lazzeri, L. Martin-Samos, N. Marzari, F. Mauri, R. Mazzarello, S. Paolini, A. Pasquarello, L. Paulatto, C. Sbraccia, S. Scandolo, G. Sclauzero, A. P. Seitsonen, A. Smogunov, P. Umari, and R. M. Wentzcovitch, "QUANTUM ESPRESSO: A modular and open-source software project for quantum simulations of materials," J. Phys.: Condens. Matter **21**, 395502 (2009).
[25]P. Giannozzi, O. Andreussi, T. Brumme, O. Bunau, M. B. Nardelli, M. Calandra, R. Car, C. Cavazzoni, D. Ceresoli, M. Cococcioni, N. Colonna, I. Carnimeo, A. D. Corso, S. de Gironcoli, P. Delugas, R. A. DiStasio, Jr., A. Ferretti, A. Floris, G. Fratesi, G. Fugallo, R. Gebauer, U. Gerstmann, F. Giustino, T. Gorni, J. Jia, M. Kawamura, H.-Y. Ko, A. Kokalj, E. Küçükbenli, M. Lazzeri, M. Marsili, N. Marzari, F. Mauri, N. L. Nguyen, H.-V. Nguyen, A. O. de-la Roza, L. Paulatto, S. Poncé, D. Rocca, R. Sabatini, B. Santra, M. Schlipf, A. P. Seitsonen, A. Smogunov, I. Timrov, T. Thonhauser, P. Umari, N. Vast, X. Wu, and S. Baroni, "Advanced capabilities for materials modelling with quantum ESPRESSO," J. Phys.: Condens. Matter **29**, 465901 (2017).
[26]M. Burkatzki, C. Filippi, and M. Dolg, "Energy-consistent pseudopotentials for quantum Monte Carlo calculations," J. Chem. Phys. **126**, 234105 (2007).
[27]J. Toulouse and C. J. Umrigar, "Optimization of quantum Monte Carlo wave functions by energy minimization," J. Chem. Phys. **126**, 084102 (2007).
[28]P. Ganesh, J. Kim, C. Park, M. Yoon, F. A. Reboredo, and P. R. C. Kent, "Binding and diffusion of lithium in graphite: Quantum Monte Carlo benchmarks and validation of van der Waals density functional methods," J. Chem. Theory Comput. **10**, 5318–5323 (2014).
[29]M. Casula, S. Moroni, S. Sorella, and C. Filippi, "Size-consistent variational approaches to nonlocal pseudopotentials: Standard and lattice regularized diffusion Monte Carlo methods revisited," J. Chem. Phys. **132**, 154113 (2010).
[30]A. Zen, S. Sorella, M. J. Gillan, A. Michaelides, and D. Alfè, "Boosting the accuracy and speed of quantum Monte Carlo: Size consistency and time step," Phys. Rev. B **93**, 241118 (2016).
[31]D. M. Ceperley and B. J. Alder, "Ground state of the electron gas by a stochastic method," Phys. Rev. Lett. **45**, 566 (1980).
[32]A. D. Becke, "Density-functional exchange-energy approximation with correct asymptotic behavior," Phys. Rev. A **38**, 3098–3100 (1988).
[33]C. Lee, W. Yang, and R. G. Parr, "Development of the Colle-Salvetti correlation-energy formula into a functional of the electron density," Phys. Rev. B **37**, 785–789 (1988).
[34]S. Grimme, "Semiempirical GGA-type density functional constructed with a long-range dispersion correction," J. Comput. Chem. **27**, 1787–1799 (2006).
[35]T. Thonhauser, S. Zuluaga, C. A. Arter, K. Berland, E. Schröder, and P. Hyldgaard, "Spin signature of nonlocal correlation binding in metal-organic frameworks," Phys. Rev. Lett. **115**, 136402 (2015).
[36]T. Thonhauser, V. R. Cooper, S. Li, A. Puzder, P. Hyldgaard, and D. C. Langreth, "Van der Waals density functional: Self-consistent potential and the nature of the van der Waals bond," Phys. Rev. B **76**, 125112 (2007).
[37]K. Berland, V. R. Cooper, K. Lee, E. Schröder, T. Thonhauser, P. Hyldgaard, and B. I. Lundqvist, "Van der Waals forces in density functional theory: A review of the VdW-DF method," Rep. Prog. Phys. **78**, 066501 (2015).
[38]S. Lehtola, C. Steigemann, M. J. T. Oliveira, and M. A. L. Marques, "Recent developments in libxc—A comprehensive library of functionals for density functional theory," SoftwareX **7**, 1–5 (2018).
[39]A. M. Rappe, K. M. Rabe, E. Kaxiras, and J. D. Joannopoulos, "Optimized pseudopotentials," Phys. Rev. B **41**, 1227–1230 (1990).
[40]G. Jeanmairet, M. Levesque, R. Vuilleumier, and D. Borgis, "Molecular density functional theory of water," J. Phys. Chem. Lett. **4**, 619–624 (2013).
[41]L. Ding, M. Levesque, D. Borgis, and L. Belloni, "Efficient molecular density functional theory using generalized spherical harmonics expansions," J. Chem. Phys. **147**, 094107 (2017).
[42]J. I. Siepmann and M. Sprik, "Influence of surface-topology and electrostatic potential on water electrode systems," J. Chem. Phys. **102**, 511–524 (1995).
[43]L. Scalfi, D. T. Limmer, A. Coretti, S. Bonella, P. A. Madden, M. Salanne, and B. Rotenberg, "Charge fluctuations from molecular simulations in the constant-potential ensemble," Phys. Chem. Chem. Phys. **22**, 10480–10489 (2020).
[44]R. Evans, "The nature of the liquid-vapour interface and other topics in the statistical mechanics of non-uniform, classical fluids," Adv. Phys. **28**, 143 (1979).
[45]J.-P. Hansen and I. McDonald, *Theory of Simple Liquids*, 3rd ed. (Academic Press, 2006).
[46]D. Borgis, S. Luukkonen, L. Belloni, and G. Jeanmairet, "Simple parameter-free bridge functionals for molecular density functional theory. Application to hydrophobic solvation," J. Phys. Chem. B **124**, 6885–6893 (2020).
[47]D. Borgis, S. Luukkonen, L. Belloni, and G. Jeanmairet, "Accurate prediction of hydration free energies and solvation structures using molecular density functional theory with a simple bridge functional," J. Chem. Phys. **155**, 024117 (2021).
[48]T. Werder, J. H. Walther, R. L. Jaffe, T. Halicioglu, and P. Koumoutsakos, "On the water-carbon interaction for use in molecular dynamics simulations of graphite and carbon nanotubes," J. Phys. Chem. B **107**, 1345–1352 (2003).
[49]J. Aqvist, "Ion-water interaction potentials derived from free energy perturbation simulations," J. Phys. Chem. **94**, 8021–8024 (1990).
[50]A. Marin-Laflèche, M. Haefele, L. Scalfi, A. Coretti, T. Dufils, G. Jeanmairet, S. Reed, A. Serva, R. Berthin, C. Bacon, S. Bonella, B. Rotenberg, P. Madden, and M. Salanne, "MetalWalls: A classical molecular dynamics software dedicated to the simulation of electrochemical systems," J. Open Source Software **5**, 2373 (2020).
[51]P. Loche, C. Ayaz, A. Schlaich, D. J. Bonthuis, and R. R. Netz, "Breakdown of linear dielectric theory for the interaction between hydrated ions and graphene," J. Phys. Chem. Lett. **9**, 6463–6468 (2018).
[52]G. Pireddu, L. Scalfi, and B. Rotenberg, "A molecular perspective on induced charges on a metallic surface," J. Chem. Phys. **155**, 204705 (2021).
[53]H. J. C. Berendsen, J. R. Grigera, and T. P. Straatsma, "The missing term in effective pair potentials," J. Phys. Chem. **91**, 6269–6271 (1987).

Supporting Information: Multi-scale simulation of the adsorption of lithium ion on graphite surface: from Quantum Monte Carlo to Molecular Density Functional Theory

Michele Ruggeri,[1] Kyle Reeves,[1] Tzu-Yao Hsu,[2] Guillaume Jeanmairet,[2] Mathieu Salanne,[1,2,3,a)] and Carlo Pierleoni[1,4,b)]

[1)] *Maison de la Simulation, CEA, CNRS, Univ. Paris-Sud, UVSQ, Université Paris-Saclay, 91191 Gif-sur-Yvette, France*

[2)] *Sorbonne Université, CNRS, Physicochimie des Électrolytes et Nanosystèmes Interfaciaux, F-75005 Paris, France*

[3)] *Institut Universitaire de France (IUF), 75231 Paris, France*

[4)] *Department of Physical and Chemical Sciences, University of L'Aquila, Via Vetoio 10, I-67010 L'Aquila, Italy*

(Dated: 13 February 2022)

[a)] Electronic mail: mathieu.salanne@sorbonne-universite.fr

[b)] Electronic mail: carlo.pierleoni@aquila.infn.it

S1. SIMULATION BOX HEIGHT CONVERGENCE

In our simulations we used periodic boundary conditions in all three dimensions; since we are interested on the adsorption on a surface we need to be sure that our simulation box is large enough in the z direction. In order to check this we examined the behavior of the DFT energy of a carbon bilayer as a function of the height of the simulation box (these DFT calculations were done using a PBE functional). We show our results in Figure S1. We can see that as we move away from the bulk case (the point with the smallest reported z, for which there is no vacuum between periodic images of the bilayer) the energy rises and quickly converges, so that at the height of 30 Å that we used the energy is well converged.

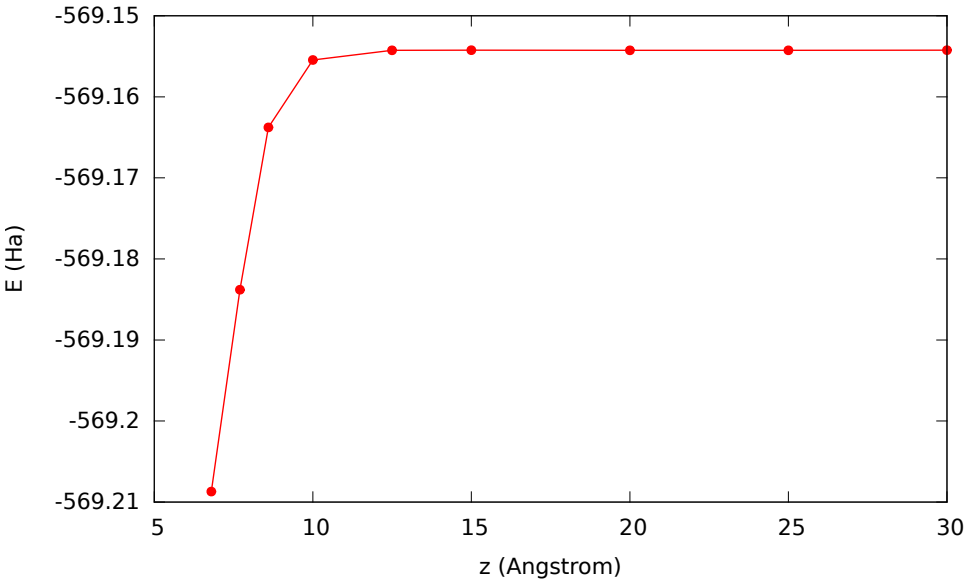

FIG. S1: DFT energy for a 5x5x1 supercell of carbon bilayer, as a function of the height z of the simulation box.

A second check was made *a posteriori* by computing the lithium adsorption profile using the vdW-DF-C09 functional and a box height of 40Å. As can be seen on Figure S2 the results with an height of 30Å and of 40Å are almost superimposed fully supporting the adequacy of our choice.

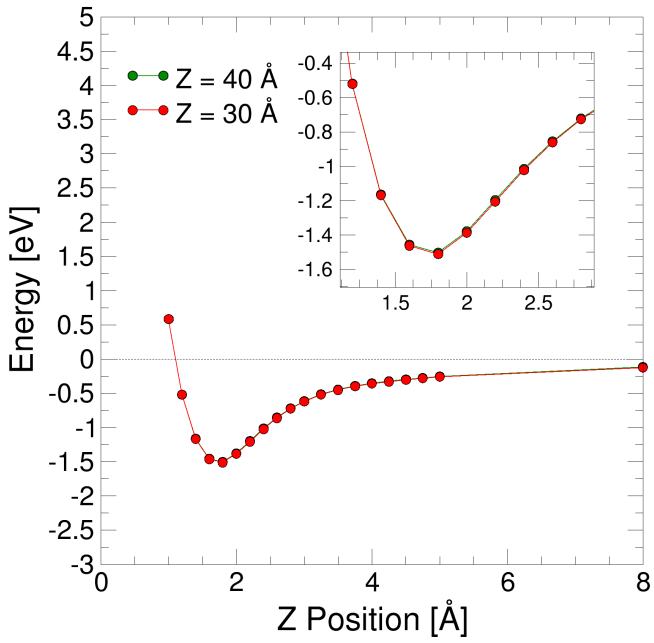

FIG. S2: Lithium adsorption energy calculated at the DFT level using the vdW-DF-C09 functional, with box heights of 30Å and 40Å.

S2. TRIAL WAVE FUNCTIONS - JASTROW TERMS

In our Quantum Monte Carlo simulations we used single determinant Slater-Jastrow trial wave functions of the form

$$\Psi_T(\mathbf{p};\mathbf{R}) = J(\mathbf{p};\mathbf{R}) \cdot D(\mathbf{R}); \tag{S1}$$

here $D(\mathbf{R})$ is a Slater determinant of single particle orbitals computed via DFT, while $J(\mathbf{p};\mathbf{R})$ is a Jastrow term describing interparticle correlations. The Slater determinant is independent on the variational parameters $\mathbf{p}$ of the trial wave function. The Jastrow term includes one and two body terms describing electrons-ions correlations, and electrons-electrons correlations respectively.

$$J(\mathbf{p};\mathbf{R}) = J^{(1)}(\mathbf{p};\mathbf{R}) \cdot J^{(2)}(\mathbf{p};\mathbf{R}) \tag{S2}$$

The one body term has the form

$$J^{(1)}(\mathbf{p};\mathbf{R}) = \exp\left[-\sum_{A}\sum_{I}^{N_A}\sum_{i}^{N_{el}} U_A(\mathbf{p};r_{Ii})\right] \tag{S3}$$

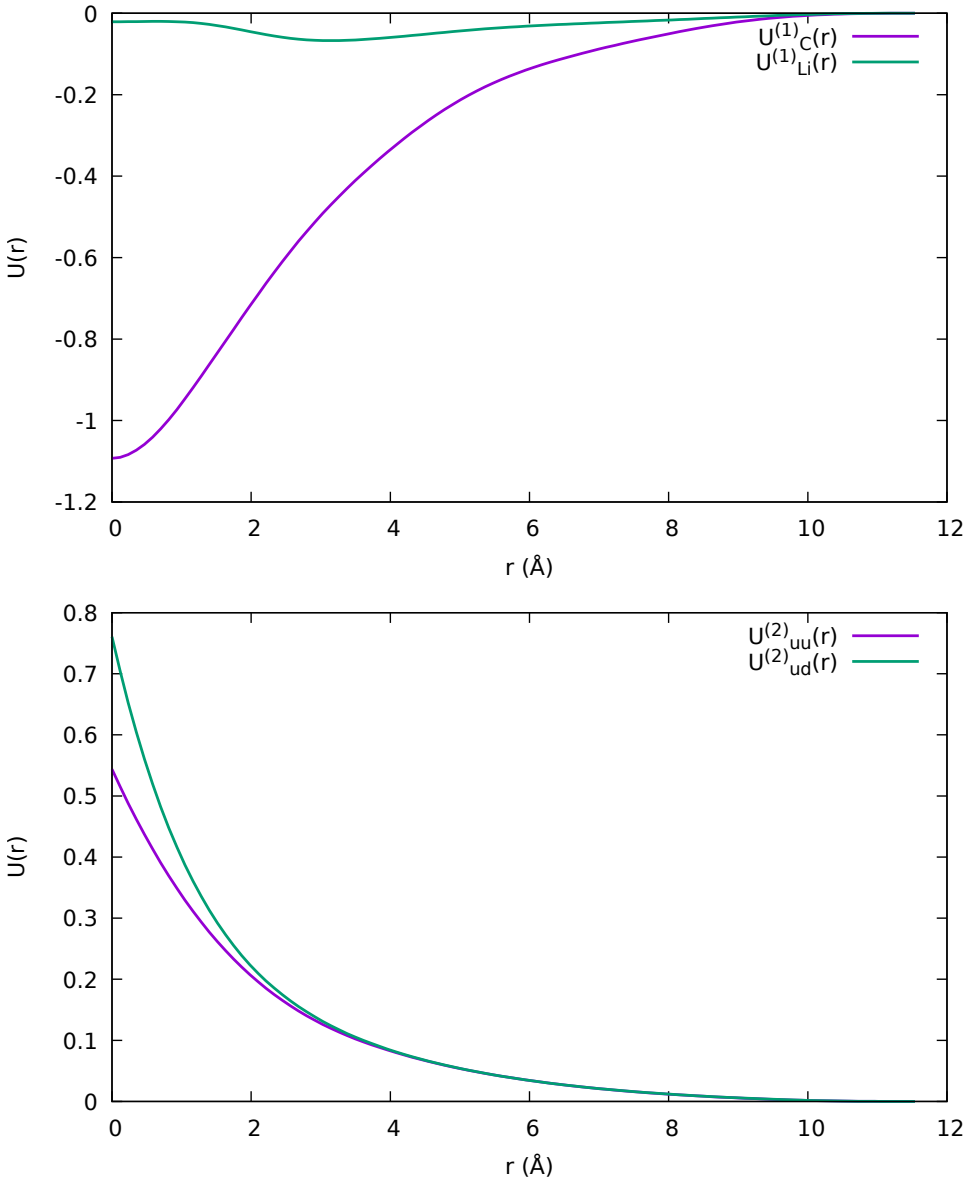

FIG. S3: Optimized pseudopotentials in the Jastrow part of a trial wave functions used to described a Li atom on a hollow adsorption site, at a distance of 2 Å from the graphite substrate; top: one body pseudopotentials describing correlations between electrons and carbon or lithium ions ($U_C^{(1)}(r)$ and $U_{Li}^{(1)}(r)$, respectively); bottom: two body pseudopotentials, describing correlations between electron with parallel ($U_{uu}^{(2)}(r)$) or antiparallel ($U_{ud}^{(2)}(r)$) spins.

where the sum over A runs over the atomic species in the simulated system; the sum over I is performed over the ions of species A, the final summation includes all electrons; the pseudopotentials $U_A(r)$, which depends only on ion-electron distances, must be numerically

optimized.

The two body term has the form

$$J^{(2)}(\mathbf{p};\mathbf{R}) = \exp\left[-\sum_{i<j}^{N_{el}} U_{s_i,s_j}(\mathbf{p};r_{ij})\right] \tag{S4}$$

here the radial pseudopotentials depends on electron spins (s_i, s_j) too: we are using different pseudopotentials for electrons pairs with parallel and antiparallel spins (U_{uu} and U_{ud} respectively).

In all cases the pseudopotentials that we used have a spline form; they are obtained interpolating a 1D B-spline on a linear grid between 0 and a distance cutoff, and the variational parameter are the values of the points to be interpolated; in our cases we always used grid with 8 points and a cutoff given by the Wigner-Seitz radius of the simulation cell.

As an example we show in Figure S3 the optimized pseudopotentials for a system composed by a Li atom on a hollow adsorption site at a distance of 2 Å from the graphite substrate.

S3. CONVERGENCE OF K-POINT MESH

A series of computations was performed to test the convergence of the total energy while varying the density of the Monkhorst-Pack grid. In each test, a lithium atom was placed at a distance of 2.4 Å from the graphite bilayer interface and positioned at the centre of a six-member ring. These tests were performed using the BLYP exchange-correlation functional. A Monkhorst-Pack grid was automatically generated by the QuantumEspresso code by specifying nk1×nk2×nk3 and displacing the grid by half a grid step. Figure S4 shows that the total energy of the system convergences quickly with the increasing density of K-points. Increasing from 1×1×1 to 2×2×1 results in a decrease of the total energy by ∼26 meV and further increasing the density from 2×2×1 to 3×3×1 results in a decrease of ∼30 meV. For computational efficiency, adsorption energy curves were computed using the 1×1×1 Monkhorst-Pack grid.

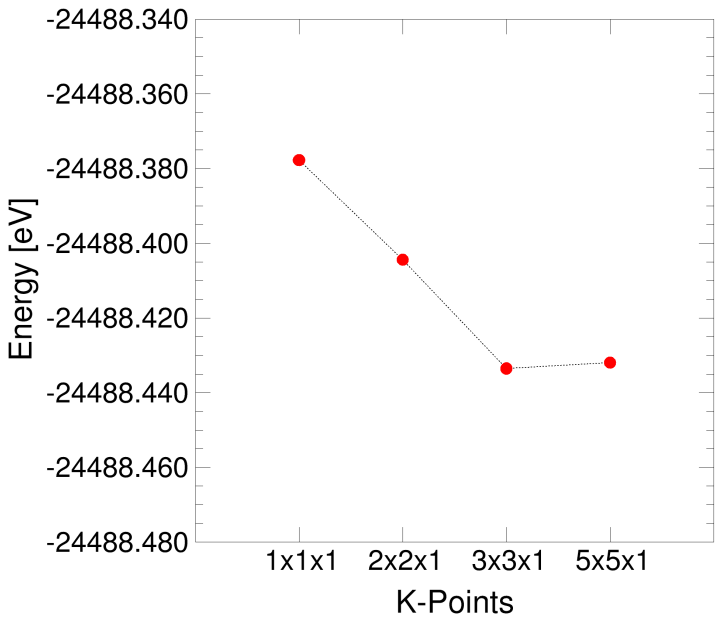

FIG. S4: The total energy (eV) computed using DFT (the XC functional is BLYP) for a system of a single lithium atom centred on six-member ring of a 10x10x1 supercell of graphite bilayer at a distance of = 2.4 Å. 1x1x1, 2x2x1, 3x3x1 and 5x5x1 Monkhorst-Pack grids were considered.

S4. INFLUENCE OF THE NUMBER OF CARBON PLANES

We computed the adsorption energy curves (with the BLYP exchange-ccorrelation functional) when including four carbon planes instead of 2. As shown on Figure S5), the adsorption energies are nearly identical on the whole range of z positions. This suggests that the including two layers is sufficient to properly describe the properties of graphite.

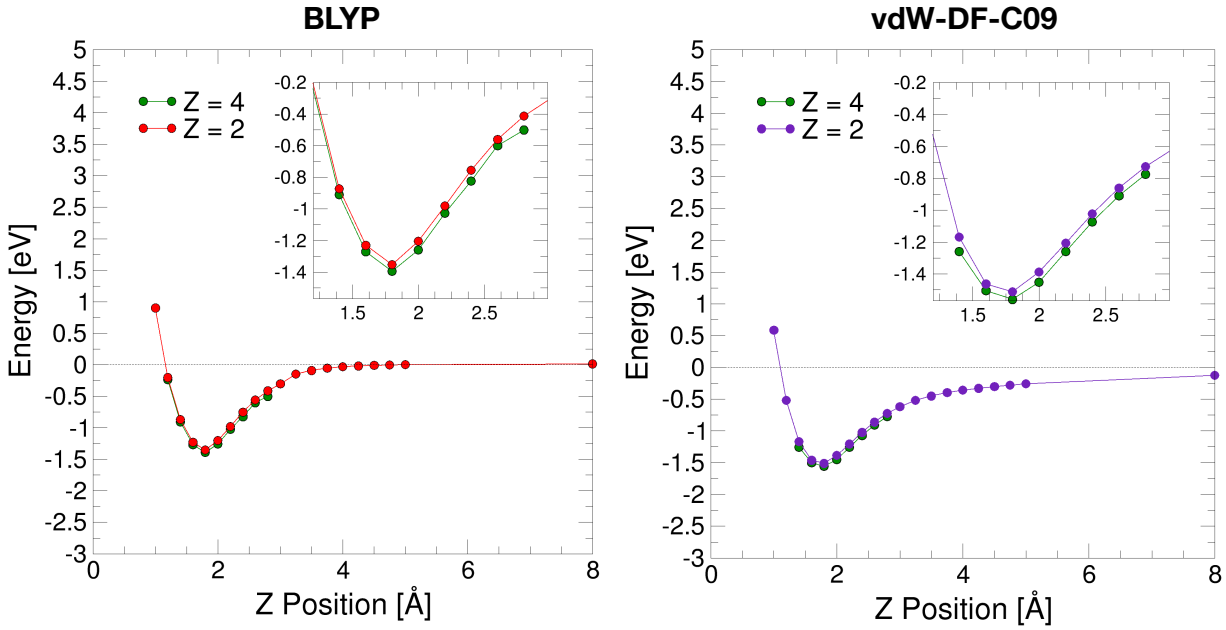

FIG. S5: Adsorption energy curves computed for two graphite layers (Z = 2, N = 100) and four graphite layers (Z = 4, N = 200). Left: BLYP; right: vdW-DF-C09. The insets show a zoomed-in version of the minimum to emphasize the similarity in the position and depth of the energy minimum.

S5. VISUALIZATION OF THE ELECTRON DENSITY FROM DFT CALCULATIONS

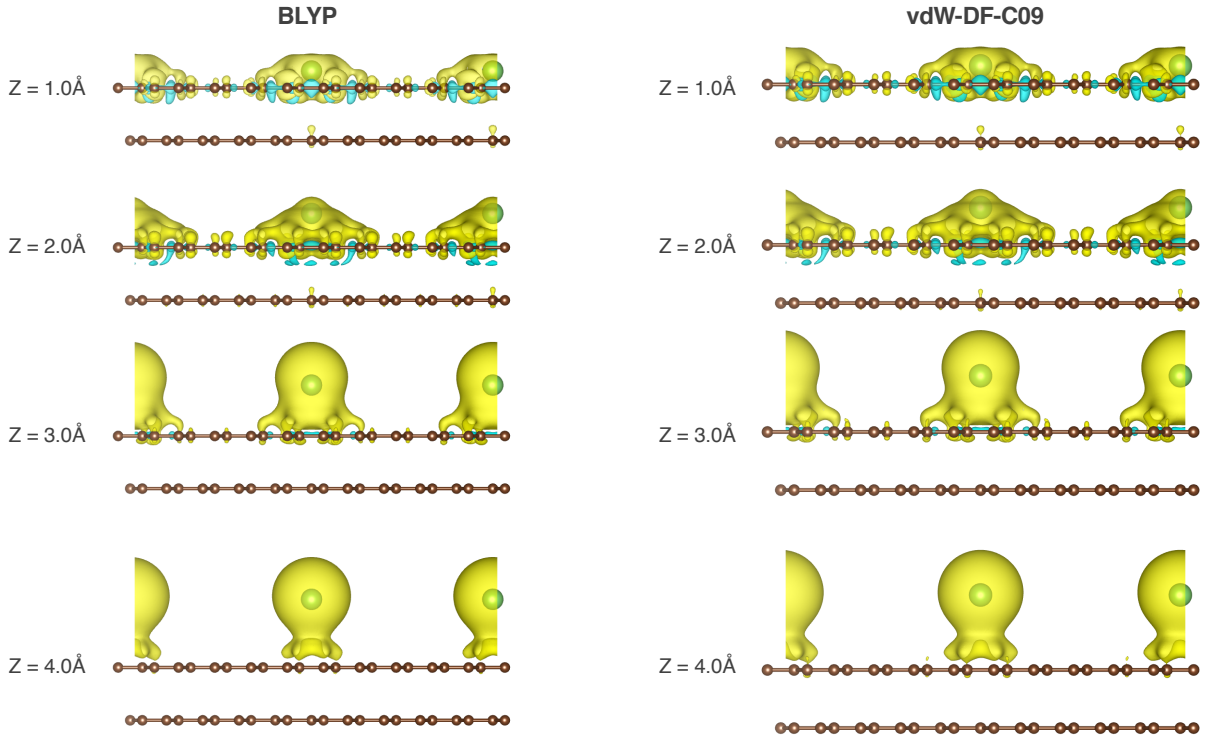

FIG. S6: Electron density around a Li atom adsorbed on a graphite substrate, computed via DFT for different atom-substrate distances (left:BLYP; right: vdW-DF-C09).